

Photon emission enhancement studies from the interaction of ultraintense laser pulses with shaped targets

S. Chintalwad , S. Krishnamurthy , and B. Ramakrishna*

Department of Physics, Indian Institute of Technology Hyderabad, Kandi, Sangareddy, 502284, India

C. P. Ridgers

Department of Physics, University of York, Heslington, York, YO10 5DD, United Kingdom

 (Received 5 July 2021; revised 12 January 2022; accepted 6 February 2022; published 22 February 2022)

We study the photon emission by bremsstrahlung and nonlinear Compton scattering from interaction of ultraintense laser pulses with cone target and flat foil using particle-in-cell simulations. The simulations are performed for laser pulses interacting with Al and Au targets. The strength of the two mechanisms of photon emission from bremsstrahlung and nonlinear Compton scattering are compared. When an ultra-intense ($I > 10^{22}$ W/cm²) laser interacts with a cone and a foil target, photon emission by bremsstrahlung is found to be comparable to that from nonlinear Compton scattering. The obtained electron energy as well as the energy and number of photons emitted were found to be higher in case of cone shaped target compared with that of a foil target. The enhanced photon emission from cone shaped target is attributed to the guiding or collimation of hot electrons towards the cone tip from the self-generated magnetic field and electrostatic field along the cone surface which pushes the hot electrons towards the tip.

DOI: [10.1103/PhysRevE.105.025205](https://doi.org/10.1103/PhysRevE.105.025205)

I. INTRODUCTION

The chirped pulse amplification (CPA) technique proposed by Strickland and Mourou provides significantly enhanced laser intensities in excess of 10^{20} W/cm² [1]. The increase in the laser intensity [2] greatly enhanced the applications of laser plasma interactions in areas like accelerator physics [3], radiography [4], radiation therapy [5], and laboratory astrophysics [6]. The increase in the laser intensity allows the electrons in the plasma to be accelerated to relativistic energies. As a result, these relativistic electrons via nonlinear processes produce radiation ranging from x rays to γ rays [7]. High sensitivity imaging such as Thomson scattering uses bright x-ray bursts, γ -ray sources are used in nuclear waste management [8,9] and γ -ray sources would also aid the development of γ - γ -ray colliders [10], which play an important role in fundamental sciences.

In ultra-intense laser-plasma interactions ($I > 10^{22}$ W/cm²), quantum electrodynamics (QED) effects play a dominant role [11,12], leading to the emission of high-energy gamma rays and pair production. Nonlinear Compton scattering and the resulting radiation reaction and pair production by the Breit-Wheeler processes [13] have been incorporated into particle-in-cell (PIC) codes like EPOCH [14] to study the QED processes in laser-plasma interactions [15–18]. When an ultra-intense laser interacts with a foil, the two main processes leading to emission of gamma rays are bremsstrahlung and nonlinear Compton scattering (NCS). Bremsstrahlung radiation is emitted when a charged particle

gets deflected or decelerated by strong electric fields of atomic nuclei. In the case of laser-plasma interactions, the photon energy depends on the intensity of the laser, target parameters like thickness, atomic number, and cross section of interaction of electron with atomic nuclei. On the other hand, in NCS, a photon γ is emitted upon collision of electron and laser photons ($e^- + n\gamma_l = e^- + \gamma$). As the gamma rays produced in this stage of the interaction play a significant role in the subsequent pair creation, it is essential to enhance the gamma ray emission in order to increase the pair production.

Recently, cone-shaped targets have attracted the interest of laser plasma community due to the advantages as in the inertial confinement fusion experiments under the fast ignition scheme. Using a cone target the laser pulse is guided into the core plasma leading to enhancement in the coupling of laser energy to the fusion pellet [19], and cone-shaped targets are used to reduce the divergence and increase the number of protons accelerated by the target normal sheath acceleration mechanism in comparison to planar targets [20]. However, the effect of the shape of the targets on the secondary photon emission processes in laser plasma interaction have not been explored to the same extent. A better understanding of the physics of cone targets is helpful with respect to the fusion-related experiments.

In this paper, we study the bremsstrahlung and nonlinear Compton scattering (NCS) radiation from cone-shaped and flat foil targets irradiated by ultra-intense laser pulses. For this study we use the open-source particle-in-cell (PIC) code EPOCH. The Monte Carlo (MC) algorithm already implemented in the EPOCH code is used to study the effects of bremsstrahlung and nonlinear Compton scattering. We study the relative strength of bremsstrahlung and nonlinear

*bhuvan@phy.iith.ac.in

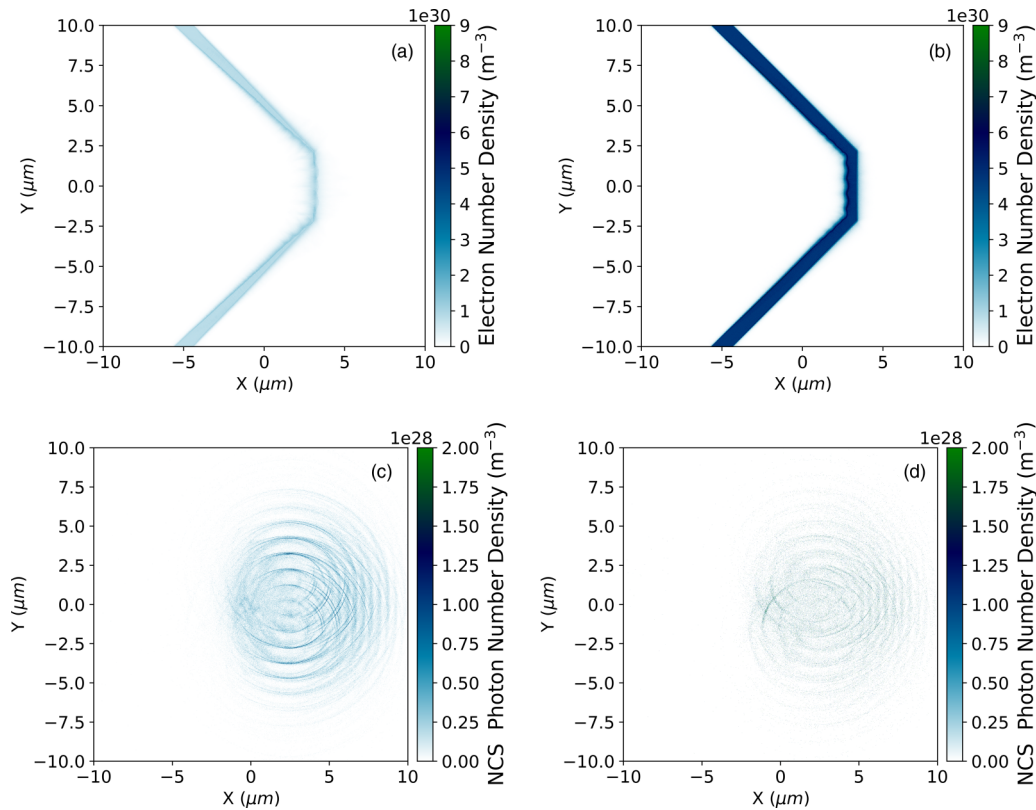


FIG. 1. (a), (b) Electron-density distribution for cone target Al (top left) and Au (top right) at $t = 0.2$ ps. (c), (d) Photon (NCS) density distribution for cone target Al (bottom left) and Au (bottom right) at $t = 75$ fs

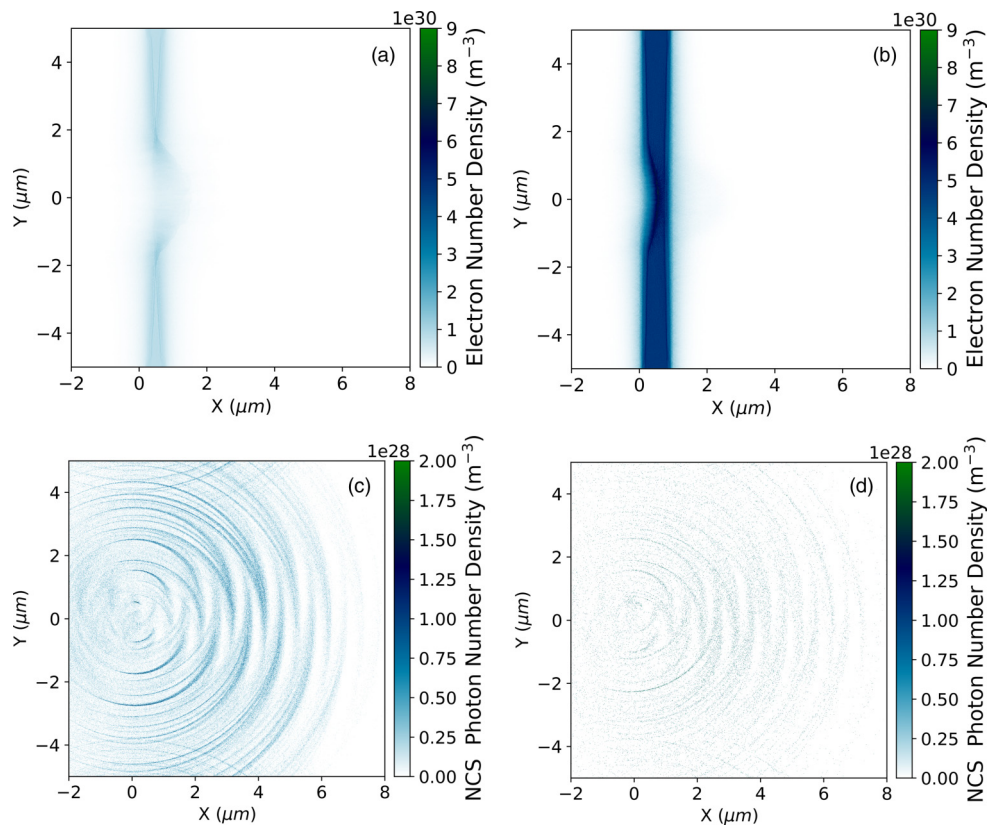


FIG. 2. (a), (b) Electron-density distribution for flat target Al (top left) and Au (top right) at $t = 0.2$ ps. (c), (d) Photon (NCS) density distribution for flat target Al (bottom left) and Au (bottom right) at $t = 40$ fs.

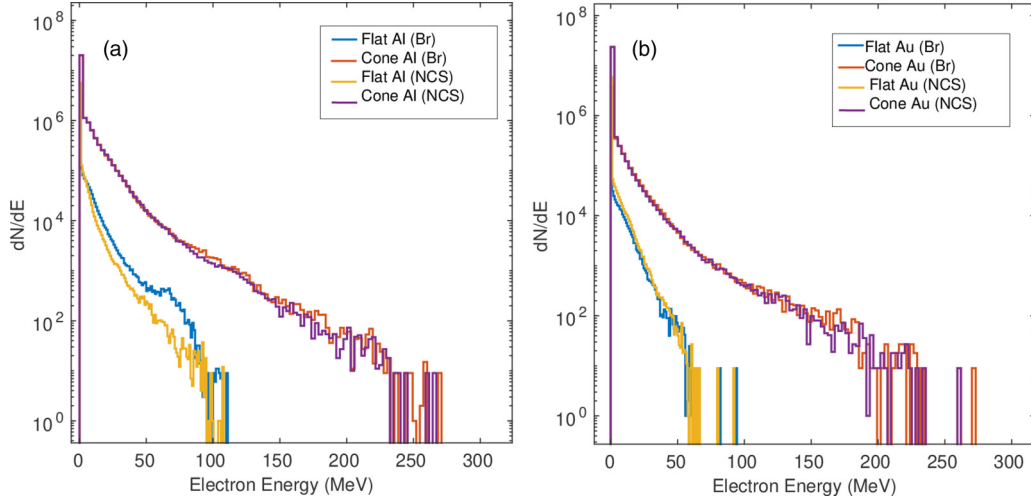


FIG. 3. (a), (b) Electron energy spectra of Al and Au for flat and cone-shaped configuration for the bremsstrahlung and NCS processes.

Compton scattering in cone targets as well as flat targets when an ultra-intense laser with intensity $I = 2 \times 10^{22} \text{ W/cm}^2$ is used to irradiate the cone and flat Al or Au target. The effect of the shape of the target as well as the Z of the target on the emission of γ rays is discussed in detail.

II. SIMULATION SETUP

We performed the simulations in the two-dimensional (2D) PIC code EPOCH. The simulation box for flat target covers $(-2 \mu\text{m} \text{ to } 8 \mu\text{m})$ along the x direction and $(-5 \mu\text{m} \text{ to } 5 \mu\text{m})$ along the y direction with 2500×2500 cells for both targets with a grid size of 4 nm. The target is placed at $x = 0 \mu\text{m}$ with $1 \mu\text{m}$ thickness. The macro particles per cell is 100 for electrons and 50 for ions. A p-polarized laser with a wavelength of $1 \mu\text{m}$ is focused to a spot with radius $1 \mu\text{m}$. The peak intensity is $2 \times 10^{22} \text{ W/cm}^2$. The laser pulse incorporated in the simulation has a Gaussian spatial and temporal profile with a pulse duration of 30 fs. The laser pulse enters the simulation box from $x = -2 \mu\text{m}$ left boundary at the start of the simulation ($t = 0$), Al or Au target has been considered as a fully ionized plasma with the electron density $n_e = 711n_c$ for Al and $n_e = 4234.4n_c$ for Au where n_c is electron critical density, $n_c = (\epsilon_0 m_e \omega_0^2) / (4\pi e^2)$, with laser frequency $\omega_0 = 2\pi c / \lambda_0$ where ϵ_0 , m_e , e , λ_0 are the permittivity of free space, the mass of the electron, the electron charge, and the laser

wavelength, respectively. The critical density corresponding to the laser wavelength $\lambda_0 = 1 \mu\text{m}$ is $n_c = 1.1 \times 10^{21} \text{ cm}^{-3}$. In all simulations we take into account only photons with energy above 50 keV. The simulation setup for cone target is also similar to the flat target except the simulation box $(-10 \mu\text{m} \text{ to } 10 \mu\text{m})$ along the x direction and $(-10 \mu\text{m} \text{ to } 10 \mu\text{m})$ along the y direction, with 5000×5000 cells for both targets. The laser is focused on the tip of the cone at $x = 2.5 \mu\text{m}$ for the cone target and at $x = 0 \mu\text{m}$ for the flat target. The tip size of the cone is $5 \mu\text{m}$ with a thickness of $1 \mu\text{m}$.

III. GAMMA-RAY EMISSION BY BREMSSTRAHLUNG AND NONLINEAR COMPTON SCATTERING

Bremsstrahlung radiation is emitted when a charged particle is deflected by another charged particle. The interaction of a high-intensity laser pulse with a solid target follows two steps: first, the generation of MeV electrons in the laser-plasma interaction [21–23]; second, conversion of these MeV electrons into MeV photons through the bremsstrahlung

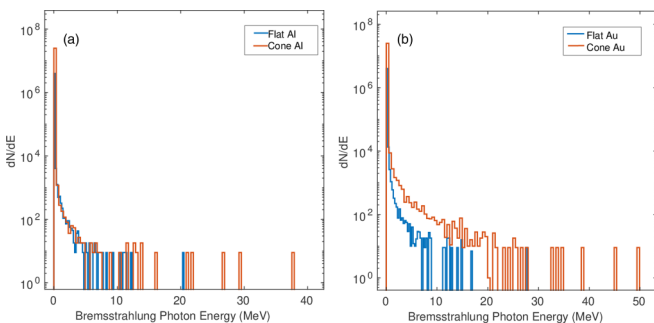


FIG. 4. (a), (b) Photon energy spectra of Al and Au for flat and cone-shaped configuration for the bremsstrahlung process.

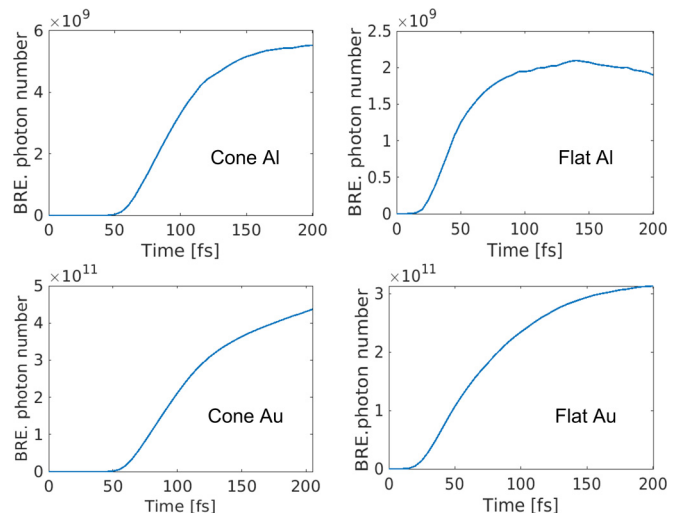


FIG. 5. Photon number in bremsstrahlung emission for flat and cone Al and Au targets.

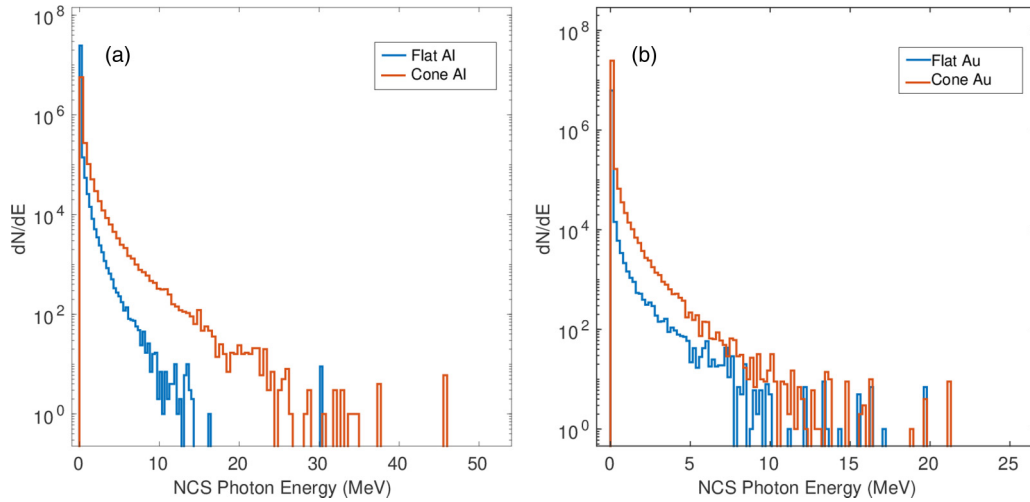


FIG. 6. (a), (b) Photon energy spectra of Al and Au for flat and cone-shaped configuration for the NCS process.

process in a high- Z solid target [24]. The bremsstrahlung radiation depends on the interaction cross section, which further depends on the Z of the target [25]. Therefore, by increasing the Z of the target, the interaction cross section also increases. On the other hand, in NCS given by the equation ($e^- + n\gamma_l \rightarrow e^- + \gamma_h$), the emission of high-energy photons depends on the interaction of target electrons (target density) with multiple laser photons (laser intensity) where γ_l is a laser photon and γ_h is an emitted high-energy photon. The strength of NCS depends on the Lorentz invariant

$$\eta = \left(\frac{\gamma}{E_s}\right)|E_{\perp} + v \times B|,$$

where γ denotes the relativistic Lorentz factor of incoming electrons in laser field, $E_s = \frac{m^2 c^3}{e\hbar}$ is the Schwinger critical field [26], and v is the incoming electron velocity. When η approaches unity, the emission becomes stochastic.

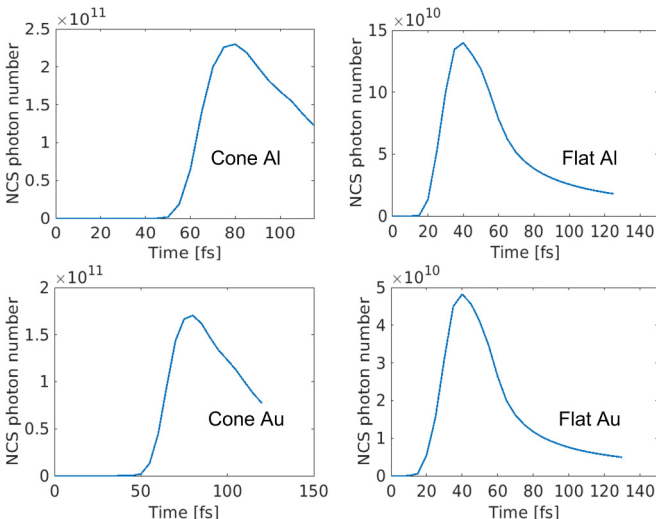


FIG. 7. The photon number in NCS emission for flat and cone Al and Au targets.

IV. RESULTS AND DISCUSSIONS

The simulation results showing the electron density and spatial distribution of photons corresponding to NCS are presented in Fig. 1 for both the Al and Au targets with cone shape at a laser intensity $I = 2 \times 10^{22}$ W/cm². The density for Al is lower than that for Au and therefore the deformation of the target is higher in the case of Al than in the case of Au. The corresponding photon density for cone-shaped Al and Au shows a higher density in case of Al than in the case of Au.

The electron density and photon emission corresponding to NCS for flat Al and Au targets is shown in Fig. 2. Obtained photon density is higher in Al target as compared with Au. The NCS photon density distribution is following the shape of the laser field.

In Fig. 3, the electron energy spectra produced by both the emission processes are shown for both Al and Au targets at $I = 2 \times 10^{22}$ W/cm² in cone and flat target configurations. The obtained maximum electron energy for cone Al_{bre} , Al_{nCS} , Au_{bre} , and Au_{nCS} target is 269, 265, 271, and 260 MeV, respectively, and the corresponding electron energy for flat Al_{bre} and Al_{nCS} is 112 and 108 MeV, respectively. For Au_{bre} and Au_{nCS} it is found to be 94 and 92 MeV, respectively. In the electron spectrum, it can be seen that the energy of electrons in the case of the cone is higher than for the flat case for both targets, and also the number of electrons in the cone target is around two orders of magnitude higher than in the flat target.

Figure 4 represents the bremsstrahlung photon energy spectra for Al and Au targets. The obtained photon energy for cone Al is higher than flat Al target and the same trend is followed by the Au target as well. The maximum photon energy for cone Al is found to be around 38 MeV, and in case of flat Al it is 20.3 MeV. For cone Au and flat Au, the obtained energy is 50 and 28 MeV, respectively. Our results are consistent with Ref. [27] for the flat target configuration.

For bremsstrahlung, the photon energy depends on the Z of the target and the intensity of the laser. Therefore, in the case of the Au target, the energy of the emitted photons by bremsstrahlung is higher compared with the Al target in both cone and flat configurations. Also, we see enhancement of the

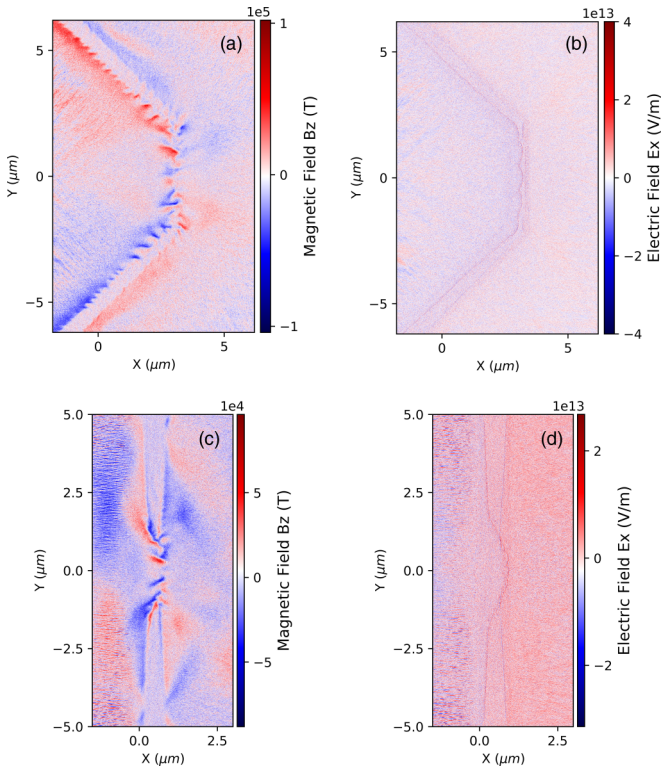


FIG. 8. (a), (b) Magnetic-field (top left) and electric-field (top right) targets for cone-shaped targets at $t = 0.15$ ps. (c), (d) Magnetic-field (bottom left) and electric-field (bottom right) targets for flat targets at $t = 0.115$ ps.

bremstrahlung photon energy in the cone target compared with that in the flat target in each material.

In support of the above observations, the photon number emitted by the bremsstrahlung mechanism is shown in Fig. 5. In our simulations, the pure photon number is obtained by taking into account the transverse size of the system, which is approximately the laser waist size ($1 \mu\text{m}$). It is found to be around 5.5×10^9 and 4.3×10^{11} for cone Al and Au, respectively. For flat targets, the obtained photon number is 2×10^9 and 3×10^{11} for Al and Au, respectively. The generated number of photons by the Al target is observed to be smaller than that for the Au target in both cone and flat

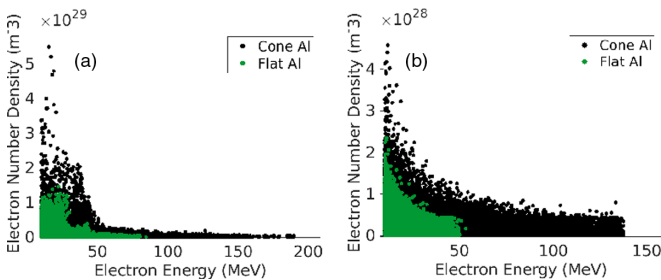


FIG. 9. (a), (b) Electron number density corresponding to their energy at the end of the laser pulse (left) and at the end of the simulation (right). Each dot represents an individual grid cell with the x coordinate being the electron energy associated with it and its corresponding electron density denoted by the y coordinate.

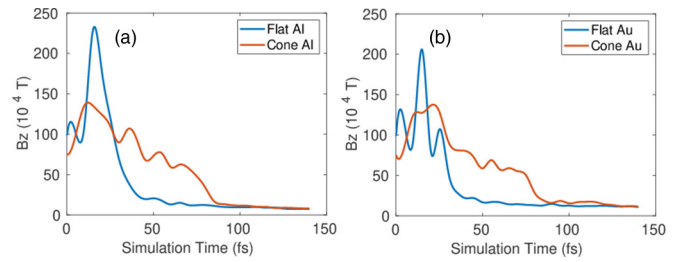


FIG. 10. (a), (b) Variation of magnetic field with time.

configurations. The maximum bremsstrahlung photon energy and the corresponding number of photons emitted are relatively higher for Au, as expected for a high- Z target. Although the electrons keep emitting bremsstrahlung photons for a longer time, we have restricted the simulations to 200 fs because the maximum energy emission occurs just after the end of laser pulse.

In the case of the NCS mechanism, the photon energy directly depends on the laser intensity and the target density. For $I = 2 \times 10^{22} \text{ W/cm}^2$, the obtained photon energy is 45.5 MeV for cone Al and 29 MeV for flat Al. For cone and flat Au the energy is 21 and 19 MeV, respectively. As seen in Fig. 6, the photon energy for NCS is high in the case of an Al target compared with a Au target and also the cone configuration gives a higher energy compared with a flat configuration in each target. The reduction of energy in the case of Au is attributed to the high density, due to which the laser cannot penetrate much deeper into the target, so the total number of electrons involved in the interaction with laser photons is reduced, resulting in reduced NCS photon yield. Guiding of fast electrons towards the cone tip increases the number of electrons in the interaction region. As indicated by the equation corresponding to the NCS mechanism ($e^- + n\gamma_I = e^- + \gamma$), the more electrons and laser photons are in the interaction region, the greater is the interaction cross section. Since the penetration depth for Al is larger, more laser photons could interact with the target electrons. The cumulative effect of guiding of electrons towards the tip of the cone and larger laser penetration depth leads to more efficient photon emission from cone targets compared with flat targets.

The number of photons emitted by the NCS mechanism is found to be 2.2×10^{11} and 1.7×10^{11} for Al and Au, respectively, in the cone configuration whereas in the flat configuration the photon number is 1.2×10^{11} and 4.8×10^{10} in Al and Au, respectively. The results imply that NCS is dominant over bremsstrahlung for low- Z targets. Also, we can see from Fig. 7 that the photon number decreases after a time step that corresponds to the end of the laser pulse in either configurations of both the targets.

As seen from the above results, irrespective of the shape of the target, the atomic number Z plays an important role in the photon emission processes. Higher Z leads to larger interaction cross section for bremsstrahlung, leading to higher bremsstrahlung emission, whereas lower Z leads to larger penetration depth for the laser, giving rise to higher NCS emission. For a particular material, we could see the enhancement in photon emission from both NCS and bremsstrahlung in case of a cone target compared with a flat target. This enhancement

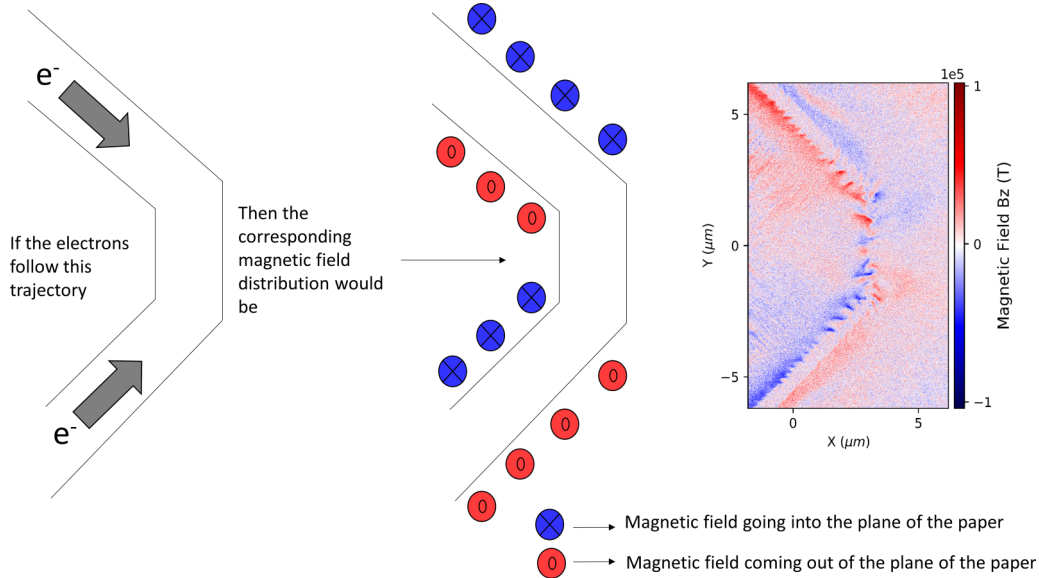


FIG. 11. Tracing of charged particles with directionality of magnetic fields at $t = 0.15$ ps.

in photon emission is due to the guiding of surface electrons from the surface of the cone towards the tip of the cone by the self-generated magnetic field and electrostatic field along the cone surface. A similar effect of magnetic and electrostatic fields on guiding of surface electrons towards the cone tip has been observed by Li *et al.* [28], Sentoku *et al.* [29], and Nakamura *et al.* [30]. Figure 8 shows the magnetic-field and corresponding electrostatic field distribution in both the configurations. The fields are generated in such a way that the electrons are confined around the tip of the cone. As a consequence of this, there is an increase in the density of electrons flowing towards the tip of the cone.

In support of the above observation, Fig. 9 plots the number of electrons with respect to the energy of electrons. In this plot, only the electrons having energy more than 10 MeV are taken into account. The figure on the left shows the snapshot taken just after the end of laser pulse and on the right is taken at the end of the simulation. The figure is shown for only the Al target, but a similar trend is followed by the Au target as well.

It is evident that the number of electrons as well as the maximum electron energy are significantly higher in the case of the cone compared with that of the flat target, implying the effect of containment from the magnetic and electrostatic field on accumulation of hot electrons.

Also, the variation of magnetic field with respect to simulation time is shown in Fig. 10. The magnetic-field decay in the case of a cone target appears to be slow whereas it decays rapidly in the case of a flat target. Since the magnetic field remains for longer duration in cone targets, it leads to more accumulation of hot electrons towards the cone tip. These observations indicate that the cone target leads to better emission of photons via both bremsstrahlung and NCS.

The depiction in the Fig. 11 shows the expected directionality of the magnetic fields generated according to the direction of flow of electrons inside the target. The figure on the right shows the magnetic field obtained from the simulation. The magnetic-field structure supports the idea that the electrons are drawn towards the tip of the cone.

This proposition is supported by the observation of electron distribution about the laser propagation direction (0°). The angular distribution of electrons is presented in Fig. 12 for both configurations. The maximum number of electrons are found along the laser propagation direction in the case of the cone target, whereas the flat target shows a relatively smaller number along the laser propagation direction, which means that the electrons in the cone target are guided toward the center. The number of electrons about the 0° direction in the case of a cone is around three times higher than that for the flat target.

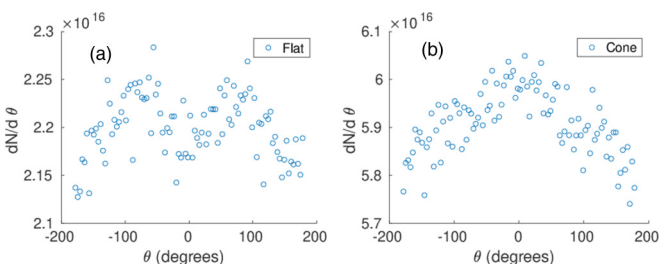


FIG. 12. (a), (b) Electron angular distribution for flat Al (left) and cone Al (right).

V. CONCLUSION

We have studied the emission of gamma rays by bremsstrahlung and nonlinear Compton scattering from the interaction of an ultrashort intense laser pulse ($I = 2 \times 10^{22}$ W/cm²) with a cone as well as a flat target via 2D EPOCH PIC simulations. The bremsstrahlung process is found to be dominant for high- Z targets whereas NCS appears as the dominant channel of radiation for low- Z targets. The bremsstrahlung and NCS processes dominate in the cone

configuration over the flat configuration for both low- Z and high- Z targets. Our study confirmed that there is enhancement in photon energy for both the radiation mechanisms when we changed the shape of the target in both low as well as high Z . The observed enhancement is mainly due to the channeling of hot electrons by the magnetic field and electrostatic field generated within the target as a result of the geometry of the cone target. Also, the generated magnetic field decays slowly in case of a cone target, thereby leading to more accumulation of hot electrons towards the tip of the cone, giving rise to about a two orders of

magnitude higher number of electrons compared with the flat target.

ACKNOWLEDGMENTS

We wish to acknowledge the EPOCH code used in this research which was developed by UK Engineering and Physics Sciences Research Council Grants No. EP/G054950/1, No. EP/G056803/1, No. EP/G055165/1 and No. EP/M022463/1. The authors also acknowledge funding from CSIR and Imprint Projects (IMP/2019/000275).

-
- [1] A. D. Strickland and G. Mourou, Compression of amplified chirped optical pulses, *Opt. Commun.* **56**, 219 (1985).
- [2] C. N. Danson *et al.*, Petawatt and exawatt class lasers worldwide, *High Power Laser Sci. Eng.* **7**, e54 (2019).
- [3] T. E. Cowan, J. Fuchs, H. Ruhl, A. Kemp, P. Audebert, M. Roth, R. Stephens, I. Barton, A. Blazevic, E. Brambrink *et al.*, Ultralow Emittance, Multi-MeV Proton Beams from a Laser Virtual-Cathode Plasma Accelerator, *Phys. Rev. Lett.* **92**, 204801 (2004).
- [4] M. D. Perry *et al.*, Hard x-ray production from high intensity laser solid interactions (invited), *Rev. Sci. Instrum.* **70**, 265 (1999).
- [5] S. V. Bulanov and V. S. Khoroshkov, Feasibility of using laser ion accelerators in proton therapy, *Plasma Phys. Rep.* **28**, 453 (2002).
- [6] S. V. Bulanov, T. Z. Esirkepov, M. Kando, J. Koga, K. Kondo, and G. Korn, On the problems of relativistic laboratory astrophysics and fundamental physics with super powerful lasers, *Plasma Phys. Rep.* **41**, 1 (2015).
- [7] K. Ta Phuoc *et al.*, All-optical Compton gamma-ray source, *Nat. Photonics* **6**, 308 (2012).
- [8] J. Magill, H. Schwoerer, F. Ewald, J. Galy, R. Schenkel *et al.*, Laser transmutation of iodine-129, *Appl. Phys. B: Lasers Opt.* **77**, 387 (2003).
- [9] E. Irani, H. Omidvar, and R. Sadighi-Bonabi, Gamma rays transmutation of Palladium by bremsstrahlung and laser inverse Compton scattering, *Energy Convers. Manage.* **77**, 558 (2014).
- [10] O. Pike, F. Mackenroth, E. Hill, and S. Rose, A photon-photon collider in a vacuum hohlraum, *Nat. Photonics* **8**, 434 (2014).
- [11] A. Di Piazza, C. Müller, K. Z. Hatsagortsyan, and C. H. Keitel, Extremely high-intensity laser interactions with fundamental quantum systems, *Rev. Mod. Phys.* **84**, 1177 (2012).
- [12] G. A. Mourou, T. Tajima, and S. V. Bulanov, More intense, shorter pulses, *Rev. Mod. Phys.* **78**, 309 (2006).
- [13] G. Breit and J. A. Wheeler, Collision of two light quanta, *Phys. Rev.* **46**, 1087 (1934).
- [14] T. D. Arber, K. Bennett, C. S. Brady, A. Lawrence-Douglas, M. G. Ramsay, N. J. Sircombe, P. Gillies, R. G. Evans, H. Schmitz, A. R. Bell, and C. P. Ridgers, Contemporary particle-in-cell approach to laser-plasma modelling, *Plasma Phys. Control. Fusion* **57**, 113001 (2015).
- [15] C. P. Ridgers, C. S. Brady, R. Ducloux, J. G. Kirk, K. Bennett, T. D. Arber, A. P. L. Robinson, and A. R. Bell, Dense Electron-Positron Plasmas and Ultraintense γ rays from Laser-Irradiated Solids, *Phys. Rev. Lett.* **108**, 165006 (2012).
- [16] C. P. Ridgers, C. S. Brady, R. Ducloux, J. G. Kirk, K. Bennett, T. D. Arber, and A. R. Bell, Dense electron-positron plasmas and bursts of gamma-rays from laser-generated quantum electrodynamic plasmas, *Phys. Plasmas* **20**, 056701 (2013).
- [17] J. G. Kirk, A. R. Bell, and I. Arka, Pair production in counter-propagating laser beams, *Plasma Phys. Control. Fusion* **51**, 085008 (2009).
- [18] S. Chintalwad, S. Krishnamurthy, B. Ramakrishna, S. Morris, and C. Ridgers, Investigation of QED effects with varying Z in thin foil targets, *IEEE Trans. Plasma Sci.* **49**, 573 (2021).
- [19] R. Kodama *et al.*, Fast heating of ultrahigh-density plasma as a step towards laser fusion ignition, *Nature (London)* **412**, 798 (2001).
- [20] D. B. Zou *et al.*, Control of target-normal-sheath-accelerated protons from a guiding cone, *Phys. Plasmas* **22**, 063103 (2015).
- [21] D. W. Forslund, J. M. Kindel, and K. Lee, Theory of Hot-Electron Spectra at High Laser Intensity, *Phys. Rev. Lett.* **39**, 284 (1977).
- [22] W. L. Kruer and K. Estabrook, $J \times B$ heating by very intense laser light, *Phys. Fluids* **28**, 430 (1985).
- [23] F. Brunel, Not-So-Resonant, Resonant Absorption, *Phys. Rev. Lett.* **59**, 52 (1987).
- [24] R. D. Edwards *et al.*, Characterization of a gamma-ray source based on a laser-plasma accelerator with applications to radiography, *Appl. Phys. Lett.* **80**, 2129 (2002).
- [25] H. W. Koch and J. W. Motz, Bremsstrahlung cross-section formulas and related data, *Rev. Mod. Phys.* **31**, 920 (1959).
- [26] J. Schwinger, On gauge invariance and vacuum polarization, *Phys. Rev.* **82**, 664 (1951).
- [27] F. Wan, C. Lv, M. Jia, H. Sang, and B. Xie, Photon emission by bremsstrahlung and nonlinear Compton scattering in the interaction of ultraintense laser with plasmas, *Eur. Phys. J. D* **71**, 236 (2017).
- [28] Y. T. Li, X. H. Yuan, M. H. Xu, Z. Y. Zheng, Z. M. Sheng, M. Chen, Y. Y. Ma, W. X. Liang, Q. Z. Yu, Y. Zhang *et al.*, Observation of a Fast Electron Beam Emitted along the Surface of a Target Irradiated by Intense Femtosecond Laser Pulses, *Phys. Rev. Lett.* **96**, 165003 (2006).
- [29] Y. Sentoku *et al.*, Laser light and hot electron micro focusing using a conical target, *Phys. Plasmas* **11**, 3083 (2004).
- [30] T. Nakamura, S. Kato, H. Nagatomo, and K. Mima, Surface-Magnetic-Field and Fast-Electron Current-Layer Formation by Ultraintense Laser Irradiation, *Phys. Rev. Lett.* **93**, 265002 (2004).